Electronic Supplementary Information

A two-dimensional mathematical model for analyzing effects of capture probe properties on the performance of lateral flow assays

Zhi Liu [a,b,*], Xiaocong He [b,c,*], Ang Li [d], Zhiguo Qu [a,#], Feng Xu [b,c,#]

[a] *Key Laboratory of Thermo-Fluid Science and Engineering of Ministry of Education, School of Energy and Power Engineering, Xi'an Jiaotong University, Xi'an 710049, P.R. China*

[b] *Bioinspired Engineering and Biomechanics Center (BEBC), Xi'an Jiaotong University, Xi'an 710049, P.R. China*

[c] *The Key Laboratory of Biomedical Information Engineering of Ministry of Education, School of Life Science and Technology, Xi'an Jiaotong University, Xi'an 710049, P.R. China*

[d] *Key Laboratory of Shaanxi Province for Craniofacial Precision Medicine Research and Department of Periodontology, College of Stomatology, Xi'an Jiaotong University, Xi'an 710004, P.R. China*

[*] *Authors contributed equally*

[#] *Corresponding authors: zgqu@mail.xjtu.edu.cn, fengxu@mail.xjtu.edu.cn*

The production rate equations

In the above concentration-governing equations, the concentration production rates $\boldsymbol{F}_{\mathbf{PA}}$, $\boldsymbol{F}_{\mathbf{RA}}$, $\boldsymbol{F}_{\mathbf{RPA}_1}$, and $\boldsymbol{F}_{\mathbf{RPA}_2}$ correspond to complexes $\mathbf{PA}$, $\mathbf{RA}$, and $\mathbf{RPA}$ in Eqs. (1-4). Based on the chemical reaction kinetics, the reagent production rates $\boldsymbol{F}_{\mathbf{PA}}$, $\boldsymbol{F}_{\mathbf{RA}}$, $\boldsymbol{F}_{\mathbf{RPA}_1}$, and $\boldsymbol{F}_{\mathbf{RPA}_2}$ correspond to Eqs. (1-4), respectively and are given as follows:

$$\boldsymbol{F}_{\mathbf{PA}} = \mathbf{k}_{\mathbf{a}} \cdot \boldsymbol{C}_{\mathbf{A}} \cdot \boldsymbol{C}_{\mathbf{P}} - \mathbf{k}_{\mathbf{d}} \cdot \boldsymbol{C}_{\mathbf{PA}} \quad \text{* MERGEFORMAT (14)}$$

$$\boldsymbol{F}_{\mathbf{RA}} = \mathbf{k}_{\mathbf{a}} \cdot \left(\mathbf{C}_{\mathbf{R}_0} - \boldsymbol{C}_{\mathbf{RA}} - \boldsymbol{C}_{\mathbf{RPA}}\right) \cdot \boldsymbol{C}_{\mathbf{A}} - \mathbf{k}_{\mathbf{d}} \cdot \boldsymbol{C}_{\mathbf{RA}} \quad \text{* MERGEFORMAT (15)}$$

$$\boldsymbol{F}_{\mathbf{RPA}_1} = \mathbf{k}_{\mathbf{a}} \cdot \left(\mathbf{C}_{\mathbf{R}_0} - \boldsymbol{C}_{\mathbf{RA}} - \boldsymbol{C}_{\mathbf{RPA}}\right) \cdot \boldsymbol{C}_{\mathbf{PA}} - \mathbf{k}_{\mathbf{d}} \cdot \boldsymbol{C}_{\mathbf{RPA}} \quad \text{* MERGEFORMAT (16)}$$

$$\boldsymbol{F}_{\mathbf{RPA}_2} = \mathbf{k}_{\mathbf{a}} \cdot \boldsymbol{C}_{\mathbf{RA}} \cdot \boldsymbol{C}_{\mathbf{P}} - \mathbf{k}_{\mathbf{d}} \cdot \boldsymbol{C}_{\mathbf{RPA}} \quad \text{* MERGEFORMAT (17)}$$

According to the nucleic acid hybridization kinetics model [33], $\mathbf{k}_a$ and $\mathbf{k}_{\mathbf{d}}$ are evaluated to be the same in the Eqs. * MERGEFORMAT (1) to * MERGEFORMAT (4). $\mathbf{k}_a$ and $\mathbf{k}_{\mathbf{d}}$ are calculated to be 3.0×10^{-5} ($\mathrm{nM^{-1}\cdot s^{-1}}$) and 1.0×10^{-7} (1/s), respectively. Furthermore, the $\boldsymbol{F}_{\mathbf{RPA}}$, which are produced by the above two approaches shown in Eqs. (16-17) are expressed as follows:

$$\boldsymbol{F}_{\mathbf{RPA}} = \boldsymbol{F}_{\mathbf{RPA}_1} + \boldsymbol{F}_{\mathbf{RPA}_2} \quad \text{* MERGEFORMAT (18)}$$

Discretization and solution procedure

The two dimensional calculation domain is discretized by using the inner node method with uniform grid spacing (**Fig. S1**). The concentration-governing equations (9)–(18) and the initial and boundary conditions Eqs. (19)–(23) are discretized by finite control volume method. The implicit scheme is applied for unsteady terms. Therefore, the discretized

concentration-governing equation of target analyte A is expressed as:

$$\frac{C_{\mathrm{A}i,j}^{\,k+1}-C_{\mathrm{A}i,j}^{\,k}}{\Delta t}=D_{\mathrm{A}}\frac{C_{\mathrm{A}i+1,j}^{\,k+1}-2C_{\mathrm{A}i,j}^{\,k+1}+C_{\mathrm{A}i\text{-}1,j}^{\,k+1}}{\Delta x^{2}}+D_{\mathrm{A}}\frac{C_{\mathrm{A}i,j+1}^{\,k+1}-2C_{\mathrm{A}i,j}^{\,k+1}+C_{\mathrm{A}i,j\text{-}1}^{\,k+1}}{\Delta y^{2}}-U\frac{C_{\mathrm{A}i+1,j}^{\,k+1}-C_{\mathrm{A}i\text{-}1,j}^{\,k+1}}{2\Delta x}-F_{\mathrm{PA}i,j}^{\,k+1} \tag{S1}$$

The discretized concentration-governing equation of report particle P is given as:

$$\frac{C_{\mathrm{P}i,j}^{\,k+1}-C_{\mathrm{P}i,j}^{\,k}}{\Delta t}=D_{\mathrm{P}}\frac{C_{\mathrm{P}i+1,j}^{\,k+1}-2C_{\mathrm{P}i,j}^{\,k+1}+C_{\mathrm{P}i-1,j}^{\,k+1}}{\Delta x^{2}}+D_{\mathrm{P}}\frac{C_{\mathrm{P}i,j+1}^{\,k+1}-2C_{\mathrm{P}i,j}^{\,k+1}+C_{\mathrm{P}i,j-1}^{\,k+1}}{\Delta y^{2}}-U\frac{C_{\mathrm{P}i+1,j}^{\,k+1}-C_{\mathrm{P}i-1,j}^{\,k+1}}{2\Delta x}-F_{\mathrm{PA}i,j}^{\,k+1} \tag{S2}$$

The discretized concentration-governing equations of complex PA are written as:

$$\frac{C_{\mathrm{PA}i,j}^{\,k+1}-C_{\mathrm{PA}i,j}^{\,k}}{\Delta t}=D_{\mathrm{P}}\frac{C_{\mathrm{PA}i+1,j}^{\,k+1}-2C_{\mathrm{PA}i,j}^{\,k+1}+C_{\mathrm{PA}i-1,j}^{\,k+1}}{\Delta x^{2}}+D_{\mathrm{P}}\frac{C_{\mathrm{PA}i,j+1}^{\,k+1}-2C_{\mathrm{PA}i,j}^{\,k+1}+C_{\mathrm{PA}i,j-1}^{\,k+1}}{\Delta y^{2}}-U\frac{C_{\mathrm{PA}i+1,j}^{\,k+1}-C_{\mathrm{PA}i-1,j}^{\,k+1}}{2\Delta x}+F_{\mathrm{PA}i,j}^{\,k+1} \tag{S3}$$

Correspondingly, the discretized balance equation of production rate of RA is given as:

$$\frac{C_{\mathrm{RA}i,j}^{\,k+1}-C_{\mathrm{RA}i,j}^{\,k}}{\Delta t}=F_{\mathrm{RA}i,j}^{\,k+1}-F_{\mathrm{RPA}_2i,j}^{\,k+1} \tag{S4}$$

The discretized balance equations of production rates of RPA are expressed as:

$$\frac{C_{\mathrm{RPA}i,j}^{\,k+1}-C_{\mathrm{RPA}i,j}^{\,k}}{\Delta t}=F_{\mathrm{RPA}i,j}^{\,k+1} \tag{S5}$$

The discretized production rates of complex PA are given as:

$$F_{\mathrm{PA}i,j}^{\,k}=\mathrm{k_a}\cdot C_{\mathrm{A}i,j}^{\,k}\cdot C_{\mathrm{P}i,j}^{\,k}-\mathrm{k_d}\cdot C_{\mathrm{PA}i,j}^{\,k} \tag{S6}$$

The discretized production rate of complex RA is written as:

$$F_{\mathrm{RA}i,j}^{\,k}=\mathrm{k_a}\cdot\left(\mathrm{C_{R_0}}-C_{\mathrm{RA}i,j}^{\,k}-C_{\mathrm{RPA}i,j}^{\,k}\right)\cdot C_{\mathrm{A}i,j}^{\,k}-\mathrm{k_d}\cdot C_{\mathrm{RA}i,j}^{\,k} \tag{S7}$$

The discretized production rates of complex RPA produced by the three methods shown in Eqs. (2c–d) are given as:

$$F_{\mathrm{RPA}_1i,j}^{\,k}=\mathrm{k_a}\cdot\left(\mathrm{C_{R_0}}-C_{\mathrm{RA}i,j}^{\,k}-C_{\mathrm{RPA}i,j}^{\,k}\right)\cdot C_{\mathrm{PA}i,j}^{\,k}-\mathrm{k_d}\cdot C_{\mathrm{RPA}i,j}^{\,k} \tag{S8}$$

$$F_{\mathrm{RPA}_2i,j}^{\,k}=\mathrm{k_a}\cdot C_{\mathrm{RA}i,j}^{\,k}\cdot C_{\mathrm{P}i,j}^{\,k}-\mathrm{k_d}\cdot C_{\mathrm{RPA_n}i,j}^{\,k} \tag{S9}$$

The discretized production rates of the total complex RPA produced by the above two methods are given as:

$$F_{\mathrm{RPA}i,j}^{\ k}=F_{\mathrm{RPA}_1 i,j}^{\ k}+F_{\mathrm{RPA}_2 i,j}^{\ k} \tag{S10}$$

Initial conditions:

$$C_{\mathrm{A}i,j}^{\ 0}=0,\ C_{\mathrm{P}i,j}^{\ 0}=0,\ C_{\mathrm{RA}i,j}^{\ 0}=0,\ C_{\mathrm{PA}i,j}^{\ 0}=0\ \&\ C_{\mathrm{RPA}i,j}^{\ 0}=0 \qquad t=0 \tag{S11}$$

Left boundary conditions:

$$C_{\mathrm{A1},j}^{\ k}=C_{\mathrm{A}_0},\ C_{\mathrm{P1},j}^{\ k}=C_{\mathrm{P}_0},\ C_{\mathrm{PA1},j}^{\ k}=0\ \mathrm{nM} \qquad x=0 \tag{S12}$$

Right boundary conditions:

$$\frac{C_{\mathrm{AL1},j}^{\ k}-C_{\mathrm{AL2},j}^{\ k}}{\Delta x}=0,\ \frac{C_{\mathrm{PL1},j}^{\ k}-C_{\mathrm{PL2},j}^{\ k}}{\Delta x}=0,\ \frac{C_{\mathrm{PAL1},j}^{\ k}-C_{\mathrm{PAL2},j}^{\ k}}{\Delta x}=0 \qquad x=L \tag{S13}$$

Up boundary conditions:

$$\frac{C_{\mathrm{A}i,M1}^{\ k}-C_{\mathrm{A}i,M2}^{\ k}}{\Delta y}=0,\quad \frac{C_{\mathrm{P}i,M1}^{k}-C_{\mathrm{P}i,M2}^{k}}{\Delta y}=0,\quad \frac{C_{\mathrm{PA}i,M1}^{\ k}-C_{\mathrm{PA}i,M2}^{\ k}}{\Delta y}=0 \qquad y=H \tag{S14}$$

Down boundary conditions:

$$\frac{C_{\mathrm{A}i,1}^{\ k}-C_{\mathrm{A}i,2}^{\ k}}{\Delta y}=0,\quad \frac{C_{\mathrm{P}i,1}^{k}-C_{\mathrm{P}i,2}^{k}}{\Delta y}=0,\quad \frac{C_{\mathrm{PA}i,1}^{\ k}-C_{\mathrm{PA}i,2}^{\ k}}{\Delta y}=0 \qquad y=0 \tag{S15}$$

The reaction rates of the complex RA, RPA_1 and RPA_2 on the fiber surface at test line are given as:

$$-D_{\mathrm{A}}\frac{C_{\mathrm{A}i,j}^{\ k}-C_{\mathrm{A}i,j-1}^{\ k}}{\Delta y}=F_{\mathrm{RA}i,j},\ -D_{\mathrm{P}}\frac{C_{\mathrm{P}i,j}^{\ k}-C_{\mathrm{P}i,j-1}^{\ k}}{\Delta y}=F_{\mathrm{RPA2}\,i,j},$$

$$-D_{P}\frac{C_{\mathrm{PA}i,j}^{\ k}-C_{\mathrm{PA}i,j-1}^{\ k}}{\Delta y}=F_{\mathrm{RPA1}i,j} \qquad x_1<x<=x_2 \tag{S15}$$

The above discretized equations are solved simultaneously with the SIMPLE algorithm [1]. As shown in **Figure S2**, the solution procedure includes the inner iteration for solving the governing and boundary equations at each time level and the outer iteration for the evolving time steps. The inner iteration is terminated until the convergence criterion of Eq. (S16) is satisfied. The convergence values then evolve to another time step for the outer iteration.

$$\max\left|\Delta C_{\mathrm{RPA}i,j}^{\ k(n)}\right|=\frac{\left[C_{\mathrm{RPA}i,j}^{\ k(n)}-C_{\mathrm{RPA}i,j}^{\ k(n-1)}\right]}{C_{\mathrm{RPA}i,j}^{\ k(\mathrm{n})}}<10^{-3} \tag{S16}$$

Numerical investigation on distribution formats of capture probe

To investigate the influence of capture probe distribution, we performed simulations by using different slope distributions of capture probes (*e.g.*, $\boldsymbol{k}=\omega(\mathbf{Y})$=1.03×10^{-7}, 7.33×10^{-8}, 2.93×10^{-8}, 0 mol/m^2 *in Eq. (25)*) to detect a series of inlet target HIV concentrations (*e.g.*, $\boldsymbol{C}_{\text{A-in}}$=1, 5, 10, 50, and 100 nM) (**Fig. S3a**). With the same slope $\boldsymbol{k}$, the signal on the top surface $\boldsymbol{S}_{\text{TOP}}$ is directly proportional to the target HIV concentration, which presents an agreement with the observation when the target HIV concentration remains a relative low value (**Fig. S3b**). With a fixed $\boldsymbol{C}_{\text{A-in}}$, a larger $\boldsymbol{k}$ will produce a higher $\boldsymbol{S}_{\text{TOP}}$, because more capture probe immobilized near the top surface of test line can provide stronger capture capacity to form **RPA**. To give an intuitive explanation, we presented the distributions of amount of **RPA** in different layers for various slope distributions of capture probes (**Fig. S3c**). Obviously, the amount of **RPA** in the top layer (13$^{\text{th}}$ layer) is increased with an increasing slope $\boldsymbol{k}$. This result indicates that $\boldsymbol{S}_{\text{TOP}}$ depends on the amount of capture probe on the top layer. In addition, $\boldsymbol{S}$ at 13$^{\text{th}}$ layer is smaller than $\boldsymbol{S}$ at 12$^{\text{th}}$ layer. This is mainly because that a relative low velocity appears at the top boundary, resulting a small amount of reagents (**A**, **PA**) passing through the region above 13$^{\text{th}}$ layer and a reduced production of **RPA**.

Reference

[1] H.J. Xu, Z.G. Qu, W.Q. Tao, Numerical investigation on self-coupling heat transfer in a counter-flow double-pipe heat exchanger filled with metallic foams, Appl Therm Eng, 66(2014) 43-54.

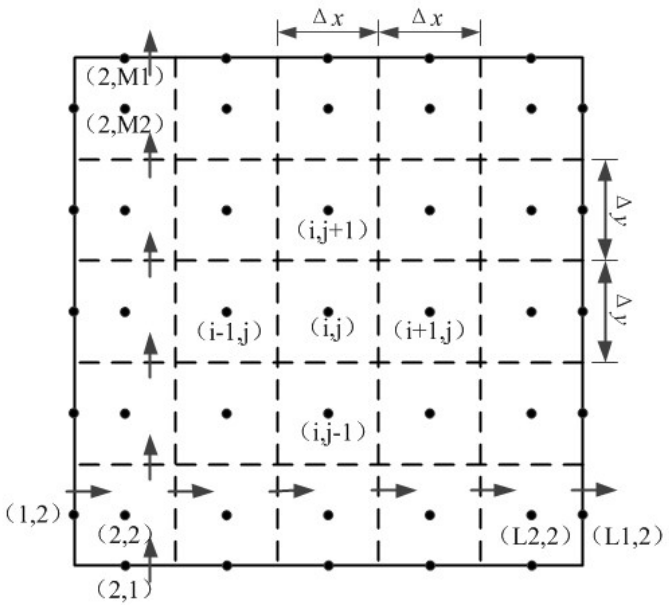

Figure S1. Spatial discretization diagram

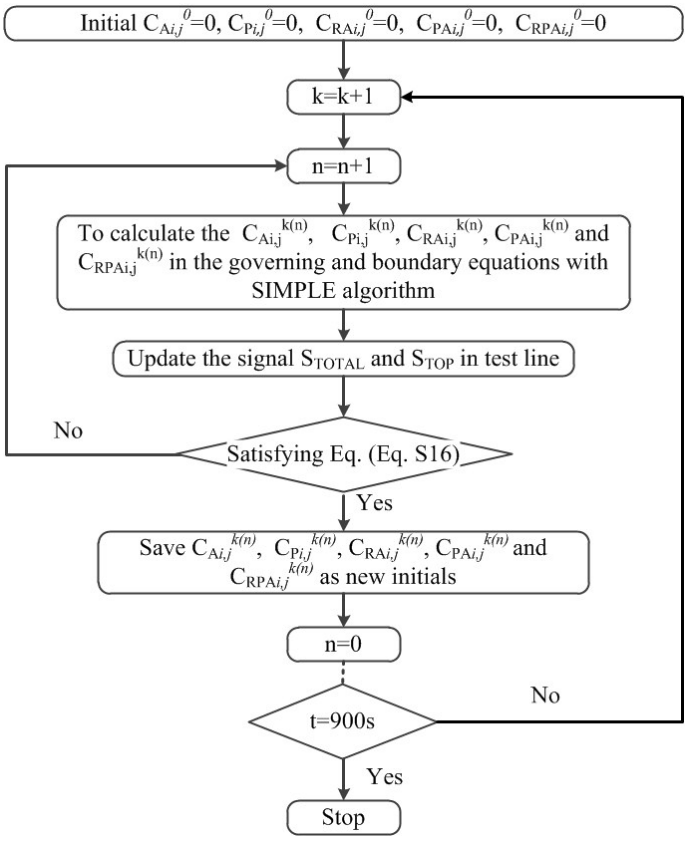

Figure S2. Solution procedure

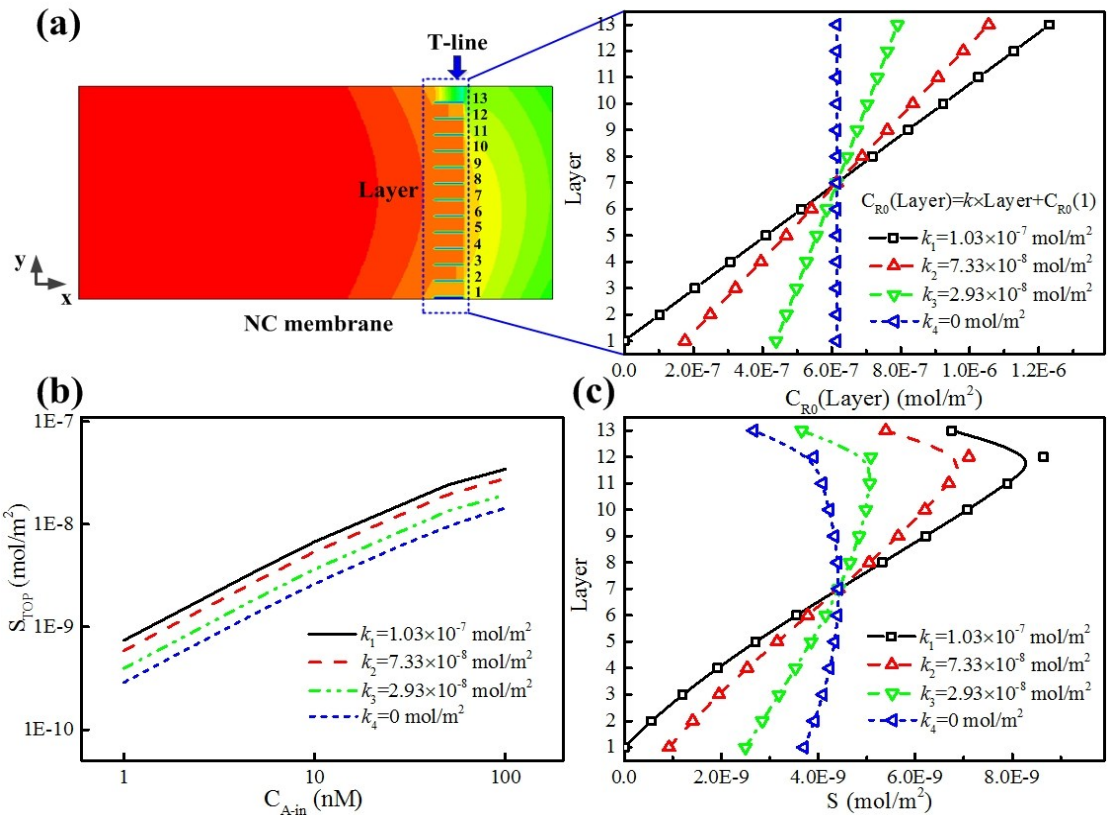

Figure S3. Numerical investigation on the effects of capture probe's distribution. (a) The capture probe distributions with various slope in thickness direction of T-line; (b) Comparison of the top signal intensity between different slopes of capture probe distributions; (c) The signal intensity in different layers under various slopes of capture probe distributions.